Introduction to Renormalization Group Theory

Jae Dong Noh

January 7, 2022

Preface

This note is prepared for the five-hours lecture in the **19th KIAS-APCTP Winter School on Statistical Physics 2022** held at APCTP, Pohang in January 10–14, 2022.

The renormalization group theory is a key to understand the scale invariance in the equilibrium and dynamical critical phenomena. It explains the reason why the critical phenomena are universal and characterized with the power laws. Moreover, it provides useful and practical tools to investigate phase transitions and critical phenomena.

The renormalization group transformation has multiple faces. The position space method using the block spin concept of Kadanoff is intuitively appealing and applicable straightforwardly to lattice systems, but less systematic. The momentum shell method is less intuitive but applicable systematically to continuous systems. The field theoretical method is powerful but highly sophisticated and least intuitive.

This lecture covers the position space and the momentum shell renormalization group theory for the equilibrium Ising model and the ϕ^4 theory. It also covers the dynamic renormalization group theory for dynamic critical phenomena of the Kardar-Parisi-Zhang equation. Finally, if time permits, we will learn how the renormalization group transformation can be assisted with numerical methods such as the Monte Carlo simulations.

The main reference of this lecture is the textbook *Lectures on phase transitions and the renormalization group* written by N. Goldenfeld [Gol92].

Contents

1

Basic concepts of renormalization group theory

1.1 Block spins

We start with the story of a **block spin** which serves as a stepping stone for the development of the renormalization group (RG) theory. Kadanoff [Kad66] proposed an interesting idea to justify the scaling ansatz of Widom [Wid65]. The block spin concept plays a central role in his idea, which makes the meaning of the scale invariance at the critical point transparent.

Consider a ferromagnetic Ising model in a d-dimensional lattice. Each lattice site i at $\boldsymbol{r}_i \in a_0\mathbb{Z}^d$ with lattice constant a_0 is occupied by an Ising spin $\sigma_i = \pm 1$. The system is close to the critical point with a small reduced temperature $\epsilon \equiv (T - T_c)/T_c$ and an external magnetic field h.

The lattice can be divided into **cells** or **blocks** of b^d sites (see Fig. 1.1). The cell size b is chosen to satisfy $ba_0 \ll \xi$ with the **correlation length** ξ. Now we will make reasonable assumptions: (i) Spins in a cell fluctuate coherently. Then, their collective states can be described by a single variable $\mu_\alpha = \pm 1$, called

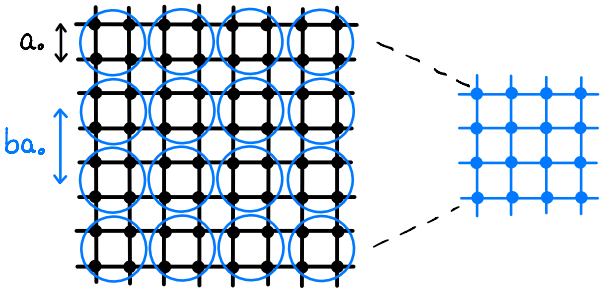

Figure 1.1: Block spin transformations with $b = 2$.

a block spin:

$$\mu_\alpha \simeq \frac{1}{b^d \langle\sigma\rangle_b} \sum_{i\in\alpha} \sigma_i, \tag{1.1}$$

where $\langle\sigma\rangle_b = \sqrt{b^{-2d} \sum_{i,j\in\alpha} \langle\sigma_i\sigma_j\rangle}$ is the magnitude of the local magnetization. The lattice constant for the block spins is $a_0' = ba_0$. (ii) Local fluctuations of spins within cells and long distance fluctuations over cells are decoupled. Then, the free energy density $f(\epsilon, h)$ is the sum of the contributions from the local spins $[f_b(\epsilon)]$ and from the block spins $[b^{-d} f(\epsilon', h')]$:

$$f(\epsilon, h) \simeq f_b(\epsilon) + b^{-d} f(\epsilon', h'). \tag{1.2}$$

The block spin has the same symmetry as the original spin. It justifies the use of the same free energy function f. The factor b^{-d} accounts for the increase of the lattice constant. The reduced temperature ϵ' and the magnetic field h' for the block spins should satisfy the constraint

$$\xi(\epsilon, h) = b\xi(\epsilon', h'). \tag{1.3}$$

Given a finite b, $f_b(\epsilon)$ should be an analytic function of ϵ and can be ignored. Likewise, ϵ' and h' should also be analytic in ϵ and h.

We can infer the information on ϵ' and h' using the power law scaling behavior near the critical point. Since $\xi(\epsilon, h = 0) \sim |\epsilon|^{-\nu}$, Eq. (1.3) implies that

$$\epsilon' = b^{y_t}\epsilon \quad \text{with} \quad y_t = 1/\nu. \tag{1.4}$$

Since the spontaneous magnetization scales as $m(\epsilon, 0) = -\left.\frac{\partial f}{\partial h}\right|_{h=0} \sim |-\epsilon|^{\beta}$, Eq. (1.2) implies that

$$h' = b^{y_h}h \quad \text{with} \quad y_h = d - \beta/\nu. \tag{1.5}$$

Kadanoff shows that the scale invariance underlies the power law scaling behavior of critical phenomena. He justifies the Widom's scaling hypothesis

$$f(\epsilon, h) \simeq b^{-d} f(b^{y_t}\epsilon, b^{y_h}h), \tag{1.6}$$

and demonstrates that the scaling from is nothing but the recursion relation of the free energy at different coupling constants linked by a scale change. Then, the following question arises: **Can we understand the critical scaling behavior by deriving the mapping between coupling constants at different length scales?** The renormalization group theory answers to this question.

1.2 Formal definition of renormalization group transformation

Consider Ising spins $\boldsymbol{\sigma} = \{\sigma_i\}$ on the d-dimensional lattice. The Hamiltonian can be written in the form

$$-\beta H[\boldsymbol{\sigma}] = \sum_n K_n \Theta_n(\boldsymbol{\sigma}), \tag{1.7}$$

where K_n's are coupling constants for operators $\Theta_0 = 1$, $\Theta_1 = \sum_i \sigma_i$, $\Theta_2 = \sum_{\langle i,j \rangle} \sigma_i \sigma_j$, and so on. We divide the lattice into cells of size b^d, and coarse-grain the system by mapping b^d spins $\boldsymbol{\sigma}_\alpha = \{\sigma_i | i \in \alpha\}$ in a cell α to a block spin μ_α. The **coarse-graining** is represented by a **conditional probability** $P_{c.g.}(\mu_\alpha | \boldsymbol{\sigma}_\alpha)$. Any choice consistent with the Z_2 **symmetry**

$$P_{c.g.}(-\mu_\alpha | -\boldsymbol{\sigma}_\alpha) = P_{c.g.}(\mu_\alpha | \boldsymbol{\sigma}_\alpha) \tag{1.8}$$

will be okay. Among others, common choices for $P_{c.g.}$ are

$$\begin{aligned} P_{c.g.}(\mu_\alpha | \boldsymbol{\sigma}_\alpha) &= \delta(\mu_\alpha, \sigma_{\alpha_0}) \qquad \textbf{[decimation]} \\ &= \delta\left(\mu_\alpha, \mathrm{sgn}\left[\sum_{i \in \alpha} \sigma_i\right]\right) \quad \textbf{[majority rule]}. \end{aligned} \tag{1.9}$$

The statistical weight of a block spin configuration $\boldsymbol{\mu} = \{\mu_\alpha\}$ is given by

$$e^{\sum_n K'_n \Theta_n(\boldsymbol{\mu})} = \mathrm{Tr}_{\boldsymbol{\sigma}} \left[\prod_\alpha P_{c.g.}(\mu_\alpha | \boldsymbol{\sigma}_\alpha)\right] e^{\sum_m K_m \Theta_m(\boldsymbol{\sigma})}. \tag{1.10}$$

This relation defines the **RG equation**

$$\boldsymbol{K}' = \boldsymbol{R}^{(b)}(\boldsymbol{K}) \tag{1.11}$$

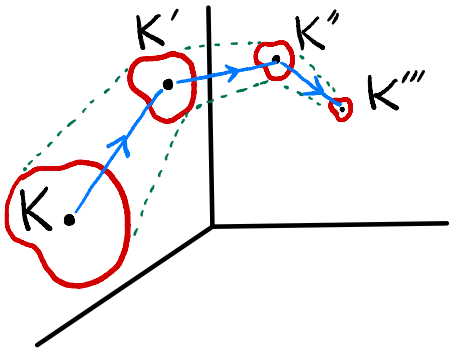

Figure 1.2: RG flow in the parameter space.

with a **map** or **flow function** $\boldsymbol{R}^{(b)}$. We add the superscript $^{(b)}$ explicitly to specify the scale factor b. Applying the RG transformation successively, one obtains a sequence $\boldsymbol{K} \to \boldsymbol{K}' \to \boldsymbol{K}'' \to \cdots$, which is called the **RG flow**. The RG transformation relates physical quantities of the system along the RG flow generated by Eq. (1.11).

To compare both systems of $\boldsymbol{\sigma}$ and $\boldsymbol{\mu}$ on the equal footing, one needs to **rescale** the length scaling. It is done by measuring the **distance in units of a lattice constant** in discrete lattices or **calibrating the distance** $r' = r/b$ in the continuum space. Thus, the correlation length decreases by the factor b: $\xi(\boldsymbol{K}') = \xi(\boldsymbol{K})/b$.

The coarse-graining and the rescaling complete the RG transformation. Figure 1.2 shows a RG flow schematically in the coupling constant parameter space. It also illustrates the change of the length scale along the RG flow. Table 1.1 summarizes the relations between the original and the renormalized systems.

Table 1.1: Transformations under the RG.

quantities	transformations
coupling constant	$\boldsymbol{K}' = \boldsymbol{R}^{(b)}(\boldsymbol{K})$
partition function	$Z'(\boldsymbol{K}') = Z(\boldsymbol{K})$
free energy density	$f(\boldsymbol{K}') = b^d f(\boldsymbol{K})$
observable $O_n = -\frac{\partial f}{\partial K_n}$	$O_n(\boldsymbol{K}') = b^d \sum_m \frac{\partial K_m}{\partial K_n'} O_m(\boldsymbol{K})$
susceptibility $\chi_{mn} = \frac{\partial^2 f}{\partial K_n \partial K_m}$	$\chi_{mn}(\boldsymbol{K}') = \cdots$
lattice constant	$a_0' = b a_0$
displacement	$\Delta \boldsymbol{r}' = b^{-1} \Delta \boldsymbol{r}$
correlation length	$\xi(\boldsymbol{K}') = b^{-1} \xi(\boldsymbol{K})$
correlation function	$C(\boldsymbol{r}'; \boldsymbol{K}') \propto C(\boldsymbol{r} = b\boldsymbol{r}'; \boldsymbol{K})$

1.3 Fixed points

The **fixed point** $\boldsymbol{K}^*$ of the RG equation is of special importance. It is determined by

$$\boldsymbol{K}^* = \boldsymbol{R}^{(b)}(\boldsymbol{K}^*). \tag{1.12}$$

The relation $\xi' = \xi/b$ implies that the correlation length at the fixed point is either 0 or ∞. A fixed point with $\xi = 0$ is called a **trivial fixed point**. It represents a **phase** of the system. On the other hand, a fixed point with $\xi = \infty$ is called the **critical fixed point** governing **critical phenomena**.

We can distinguish the trivial and critical fixed points with the **linear stability analysis**. In the vicinity of a fixed point $\boldsymbol{K}^*$, the RG equation for $\delta\boldsymbol{K} = \boldsymbol{K} - \boldsymbol{K}^*$ can be linearized

$$\delta\boldsymbol{K}' = \boldsymbol{\Lambda}^{(b)} \cdot \delta\boldsymbol{K} \tag{1.13}$$

with a linear RG transformation matrix $\boldsymbol{\Lambda}^{(b)}$. Diagonalizing $\boldsymbol{\Lambda}^{(b)}$, we can rewrite Eq (1.13) in the form

$$\begin{pmatrix} u_1' \\ u_2' \\ \vdots \end{pmatrix} = \begin{pmatrix} b^{y_1} & & \\ & b^{y_2} & \\ & & \ddots \end{pmatrix} \begin{pmatrix} u_1 \\ u_2 \\ \vdots \end{pmatrix}, \tag{1.14}$$

where u_n and y_n are called a **scaling variable** and a **scaling dimension**, respectively. There are three types of scaling variables:

- $y_n > 0$: u_n is a **relevant** scaling variable. The fixed point is **unstable** in this direction.
- $y_n < 0$: u_n is an **irrelevant** scaling variable. The fixed point in **stable** in this direction.

- $y_n = 0$: u_n is a **marginal** scaling variable. It may be truly marginal, marginally relevant, or marginally irrelevant.

In terms of scaling variables, the free energy transforms as

$$f(u_1, u_2, \cdots, u_n, \cdots) = b^{-d} f(b^{y_1} u_1, b^{y_2} u_2, \cdots, b^{y_n} u_n, \cdots). \tag{1.15}$$

It suffices to consider only relevant scaling variables because irrelevant scaling variables vanish in the large b limit (unless there exist *dangerously irrelevant* scaling variables).

A magnetic system usually has *two* relevant scaling variables: a **reduced temperature** $u_1 = \epsilon$ with y_t and a **magnetic field** $u_2 = h$ with y_h. Thus, the free energy satisfies the Widom scaling form

$$f(\epsilon, h) \simeq b^{-d} f(b^{y_t}\epsilon, b^{y_h} h). \tag{1.16}$$

All the **critical exponents** are determined by the scaling dimensions of relevant scaling variables.

The coupling constant can flow into a critical fixed point along the irrelevant directions. The basin of attraction of a critical fixed point is called the **critical manifold**. It corresponds to the **phase boundary** separating phases at either side.

1.4 RG flow and phase diagram

We illustrate typical RG flows for Ising-type systems in Fig. 1.4. Figure 1.4 (b) is for the Ising model with nearest and next nearest neighbor interactions with strength $K_{nn} = \beta J_{nn}$ and $K_{nnn} = \beta J_{nnn}$. The critical fixed point has a relevant direction and an irrelevant direction. The irrelevant direction defines a critical manifold. Given J_{nn} and J_{nnn}, the model moves along a line as the inverse temperature $\beta = 1/(k_B T)$ varies. Such a line is called a **physical line**. A phase transition takes place

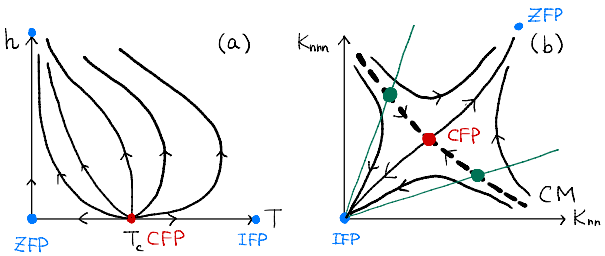

Figure 1.3: Typical RG flows of Ising systems in the (T, h) plane (a) and in the (K_{nn}, K_{nnn}) plane (b). The zero-temperature fixed point (ZFP) and the infinite-temperature fixed point (IFP) are the trivial fixed points with $\xi = 0$. They represent the paramagnetic and the ferromagnetic phases, respectively. The critical manifold (CM) is drawn with a dashed line in (b). It is the phase boundary separating the ferromagnetic phase and the paramagnetic phase.

when the physical line crosses the critical manifold. The critical behavior is governed by the critical fixed point into which the critical manifold flows. Note that any models with different ratio J_{nnn}/J_{nn} display the same critical behavior. This example hints a reason why critical phenomena are classified to the **universality class**.

2

Position space RG for Ising models

We will exercise the RG transformation for the Ising model on discrete lattices. In the following examples, the RG transformation can be done exactly owing to the special properties of the underlying lattice structure. We warn that the RG transformation can be done only approximately in most cases.

2.1 1-d Ising spin chain

The Hamiltonian of the 1-d Ising spin chain is given by

$$\mathcal{H}[\boldsymbol{\sigma}] \equiv \beta H = -K \sum_{i \in \mathbb{Z}} \sigma_i \sigma_{i+1} - h \sum_{i \in \mathbb{Z}} \sigma_i, \tag{2.1}$$

where $K = \beta J$ and $h = \beta h_0$.

We coarse-grain the system with a scale factor $b = 2$ by replacing a pair of spins $(\sigma_{2i}, \sigma_{2i+1})$ with a block spin $\mu_i = \sigma_{2i}$ [decimation]. Note that decimated spins (blue filled circles in Fig. 2.1) do not interact with other decimated spins. Thus, the partial trace over $\{\sigma_{2i+1}\}$ can be taken independently. The

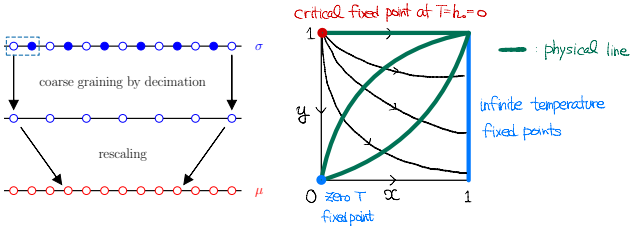

Figure 2.1: RG transformation of the 1d Ising spin chain and the RG flow. The green lines are physical lines.

RG equation is derived from

$$e^{K'\mu\mu'+h'(\mu+\mu')/2} = c \sum_{\sigma=\pm 1} e^{K\sigma(\mu+\mu')+h(\sigma+(\mu+\mu)/2)}. \tag{2.2}$$

In terms of $x = e^{-4K}$ and $y = e^{-2h}$, we obtain

$$x' = x\frac{(1+y)^2}{(x+y)(1+xy)}, \quad y' = y\frac{x+y}{1+xy}. \tag{2.3}$$

It has a critical fixed point at $(x^*, y^*) = (0, 1)$ with $T = h = 0$. Thus, the 1d Ising spin system is in the paramagnetic disordered phase at any finite temperatures.

2.2 Ising model on a hierarchical lattice

The Ising model on a hierarchical lattice is also solved exactly by using the RG transformation [KG81]. The hierachical lattice is generated iteratively as shown in Fig. 2.2. Due to the hierarchical structure, decimation by reversing the iteration leads to the exact RG transformation. Decimated spins do not interact

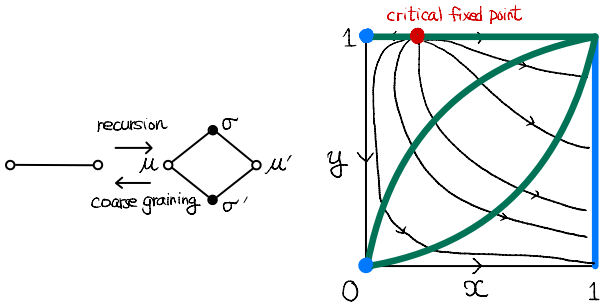

Figure 2.2: Recursive rule for a hierarchical lattice and the RG flow. The green lines are physical lines.

with each other. Thus, the coarse-graining is done trivially as in the 1d Ising model. In terms of $x \equiv e^{-4K}$ and $y = e^{-2h}$, the RG equation is given by

$$x' = x^2 \frac{(1+y)^4}{(x+y)^2(1+xy)^2}, \quad y' = y\frac{(x+y)^2}{(1+xy)^2}. \tag{2.4}$$

The RG flow is drawn schematically in Fig. 2.2. There is a critical fixed point at $(x_c, 1)$ where x_c is determined with $(1+x_c)^4 = 16x_c$. It governs the critical behavior of the spontaneous symmetry breaking transition. Near the critical fixed point, the RG equation can be linearized as $\delta x' = \Lambda_t \delta x$ and $\delta y' = \Lambda_h \delta y$ with $\Lambda_t = 1.67857\ldots = \Lambda_h - 1$. Decimation reduces the number of total sites by factor $\tilde{b} = 4$. The scaling dimensions of the temperature-like scaling variable δx and of the magnetic-field-like scaling variable δy are $y_t = \ln \Lambda_t / \ln \tilde{b} = 0.373616\ldots$ and $y_h = \ln \Lambda_h / \ln \tilde{b} = 0.710731\ldots$. The exponent $\tilde{\nu} = 1/y_t$ is then interpreted as a **correlation volume exponent**.

3 Dynamical RG Theory

In this chapter, we will learn how to study long time and long distance scaling behavior of a dynamical system using the RG theory. A dynamical system is defined by an equation of motion, which is specified by a set of parameters $\boldsymbol{K}$. The **dynamic RG** tranformation means the **coarse-graining** of the length scale by a factor of b and the time scale by a factor of b^z followed by the **rescaling**. The resulting effective equation of motion allows us to find the RG flow equation $\boldsymbol{K}' = R_b(\boldsymbol{K})$. The asymptotic scaling behavior is also obtained from the **fixed points** of the RG flow. To be concrete, we explain all the details of the dynamic RG for the model system of the **Kardar-Parisi-Zhang (KPZ)** equation.

3.1 Kardar-Parisi-Zhang equation

The KPZ equation [KPZ86] describes the stochastic growth of an interface over a d-dimensional substrate. The interface height $h(\boldsymbol{r} \in \mathbb{R}^d, t) \in \mathbb{R}$ follows

$$\frac{\partial h}{\partial t} = \nu \nabla^2 h + \frac{\lambda}{2} |\nabla h|^2 + \eta(\boldsymbol{r}, t), \tag{3.1}$$

where $\eta(\boldsymbol{r},t)$ is a Gaussian white noise characterized by

$$\langle \eta(\boldsymbol{r},t)\rangle = 0,\ \langle \eta(\boldsymbol{r},t)\eta(\boldsymbol{r}',s)\rangle = D\delta(\boldsymbol{r}-\boldsymbol{r}')\delta(t-s) \tag{3.2}$$

with the noise strength D. The KPZ equation with colored noises is studied in [MHKZ89]. The KPZ equation is specified by the parameter set $\boldsymbol{K} = \{\nu, D, \lambda\}$.

Starting from the flat initial configuration $h(\boldsymbol{r},0) = 0$, the interface roughens satisfying the dynamic scaling

$$\left\langle (h(\boldsymbol{r},t) - h(\boldsymbol{r}',t))^2 \right\rangle \sim \begin{cases} |\boldsymbol{r}-\boldsymbol{r}'|^{2\chi}, & |\boldsymbol{r}-\boldsymbol{r}'| \ll t^{1/z} \\ t^{2\chi/z}, & |\boldsymbol{r}-\boldsymbol{r}'| \gg t^{1/z} \end{cases} \tag{3.3}$$

where χ is the **roughness exponent** and z is the **dynamic exponent**. The spatial growth of the interface fluctuations is described by the roughness exponent χ and the temporal growth by the growth exponent χ/z. The dynamic exponent z describes the relation between the time scale and the length scale, $\tau \sim \xi^z$.

When the **nonlinear** or **KPZ** term λ is equal to zero, Eq. (3.1) reduces to the linear **Edwards-Wilkinson (EW)** equation. In the linear theory, the exponents take the values $\chi = \chi_{EW} = (2-d)/2$ and $z = z_{EW} = 2$. We will investigate the effect of the KPZ term using the RG.

3.2 Power counting

It is instructive to perform the **naive power counting** or **dimensional analysis**. It corresponds to the RG transformation without coarse-graining. Consider a rescaled field $h'(\boldsymbol{r},t)$ that is a reduced copy of the original field:

$$h(\boldsymbol{r},t) \to h'(\boldsymbol{r},t) = b^{-\chi}\, h(b\boldsymbol{r}, b^z t) \tag{3.4}$$

with a scale factor $b > 1$. The reduction ratios for the length scale and the time scale are different in general. The rescaled field follows the equation of motion

$$\begin{aligned} b^{\chi-z}\frac{\partial h'}{\partial t} &= b^{\chi-2}\nu\nabla^2 h' + b^{2\chi-2}\frac{\lambda}{2}|\nabla h'|^2 + \eta(b\boldsymbol{r}, b^z t) \\ \frac{\partial h'}{\partial t} &= b^{z-2}\nu\nabla^2 h' + b^{\chi+z-2}\frac{\lambda}{2}|\nabla h'|^2 + b^{z-\chi}\eta(b\boldsymbol{r}, b^z t). \end{aligned} \tag{3.5}$$

This form is identical to the original KPZ equation with the modified parameters

$$\nu' = b^{z-2}\nu, \quad D' = b^{z-2\chi-d}D, \quad \lambda' = b^{\chi+z-2}\lambda\ . \tag{3.6}$$

Note that the rescaled noise $\eta'(\boldsymbol{r}, t) = b^{z-\chi}\eta(b\boldsymbol{r}, b^z t)$ is also a Gaussian white noise, whose strength D' follows from

$$\left\langle \eta'(\boldsymbol{r}, t)\eta'(\boldsymbol{r}', s)\right\rangle = b^{z-2\chi-d}D\delta(\boldsymbol{r}-\boldsymbol{r}')\delta(t-s). \tag{3.7}$$

The power counting confirms that the EW equation is **scale-invariant** ($v' = v$, $D' = D$, $\lambda' = \lambda = 0$) with the choice of $z = z_{EW}$ and $\chi = \chi_{EW}$. Plugging the EW exponents into (3.6), one obtains that $\lambda' = b^{\chi_{EW}-z_{EW}-2}\lambda = b^{1-d/2}\lambda$. When $d < 2$, a nonzero λ grows indefinitely as b increases. It implies that the nonlinear term is a **relevant** perturbation to the EW equation for $d < 2$. The simple power counting fails to predict the scaling exponents of the KPZ equation for $d < 2$, which calls for the RG approach.

3.3 KPZ equation in the Fourier space and diagram representation

It is convenient to work in the Fourier space with wavevector $\boldsymbol{k} \in \mathbb{R}^d$ and angular frequency ω. For simplicity, we introduce a *momentum variable* $\mathsf{p} = (\boldsymbol{k}, \omega)$ and a shorthand notation

$$\int đ\mathsf{p} \equiv \iint đ\boldsymbol{k} đ\omega \equiv \iint \frac{d^d\boldsymbol{k}}{(2\pi)^d}\frac{d\omega}{2\pi}. \tag{3.8}$$

The Fourier and inverse Fourier transformations are defined as

$$\begin{aligned} h(\mathsf{p}) &= \iint d^d\boldsymbol{r}dt\; h(\boldsymbol{r},t)e^{-i(\boldsymbol{k}\cdot\boldsymbol{r}-\omega t)} \\ h(\boldsymbol{r},t) &= \int đ\mathsf{p}\; h(\mathsf{p})e^{i(\boldsymbol{k}\cdot\boldsymbol{r}-\omega t)}. \end{aligned} \tag{3.9}$$

The KPZ equation in the Fourier space becomes

$$\begin{aligned} h(\mathsf{p}) &= G_0(\mathsf{p})\eta(\mathsf{p}) \\ &\quad - \frac{\lambda}{2}G_0(\mathsf{p})\int đ\mathsf{p}'\left(\frac{k^2}{4}-k'^2\right)h\left(\frac{\mathsf{p}}{2}-\mathsf{p}'\right)h\left(\frac{\mathsf{p}}{2}+\mathsf{p}'\right), \end{aligned} \tag{3.10}$$

where

$$G_0(\mathsf{p}) \equiv \frac{1}{\nu k^2 - i\omega} \tag{3.11}$$

is called the **free propagator**. The noise in the Fourier space $\eta(\mathsf{p})$ has the correlator

$$\langle \eta(\mathsf{p})\eta(\mathsf{p}')\rangle = D\,\bar{\delta}(\mathsf{p}+\mathsf{p}'), \tag{3.12}$$

where

$$\bar{\delta}(\mathsf{p}+\mathsf{p}') \equiv (2\pi)^{d+1}\delta(\boldsymbol{k}+\boldsymbol{k}')\delta(\omega+\omega'). \tag{3.13}$$

One can handle the algebraic relations conveniently by using a **diagram method**. We introduce the following rules:

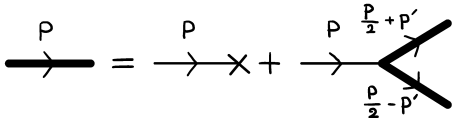

Figure 3.1: Diagram representation of the KPZ equation.

- (**Thick line**) = $h(\mathsf{p})$, (**thin line**) = $G_0(\mathsf{p})$, and ($\times$ **symbol**) = $\eta(\mathsf{p})$. They are assigned to a momentum variable.
- (**3-vertex** associated with an incoming momentum p and two outgoing momenta p_1 and p_2) = $\int đ\mathsf{p}_1 đ\mathsf{p}_2 \left(-\frac{\lambda}{2}\right) (\boldsymbol{k}_1 \cdot \boldsymbol{k}_2)\, \delta(\mathsf{p} - \mathsf{p}_1 - \mathsf{p}_2)$.

The diagram representation of the KPZ equation is shown in Fig. 3.1.

We introduce additional rules to represent the noise average.

- (**Empty circle** $\circ$ associated with two momentum variables p and p') = $D\, \delta(\mathsf{p} + \mathsf{p}')$. This symbol replaces the average of the product of two noise variables [**constraction**]. Equation (3.12) can be written as

$$\langle \times_{\mathsf{p}} \times_{\mathsf{p}'} \rangle = \circ_{\mathsf{p},\mathsf{p}'} \tag{3.14}$$

  where the subscripts are added to specify associated momenta and can be omitted.

- The noises are Gaussian distributed. Thus, the contraction of multiple noise variables follows from the **Wick's theorem**. For example,

$$\langle \times_1 \times_2 \times_3 \times_4 \rangle = \circ_{1,2} \circ_{3,4} + \circ_{1,3} \circ_{2,4} + \circ_{1,4} \circ_{2,3}\,. \tag{3.15}$$

3.4 Momentum shell RG transformation

The momentum shell RG transformation with a scale factor $b > 1$ proceeds in the following way [MM75] (see also Fig. 3.2):

1. **Momentum shell**: Introduce an **ultraviolet cutoff** Λ and assume that $|\boldsymbol{k}| < \Lambda$. Its inverse corresponds to a lattice constant $a_0 = 2\pi/\Lambda$ of a lattice system. The momentum shell $\partial\Lambda$ is the region where $\Lambda/b < |\boldsymbol{k}| < \Lambda$. We will use a subsrcipt $_{>(<)}$ to specify that a quantity is associated with a long wavelength wavevector ($\boldsymbol{k} \in \hat{\phi}\Lambda$) or a short wavelength wavevector ($\boldsymbol{k} \in \partial\Lambda$).

2. **Coarse-graining**: Solve the equation of motion to obtain $h_>$ in terms of $h_<$ and η. **Eliminating** $h_>$ from the equation of motion and **averaging over** $\eta_>$ the remaing terms, one can obtain the effective equation of motion for $h_<$ with a renormalized parameter $\boldsymbol{K}' = \{\nu', D', \lambda'\}$.

3. **Rescaling**: Rescale the momentum and the field variables to define the renormalized field

$$h_R(\boldsymbol{k}, \omega) = b^{-\chi}\, h_<(\boldsymbol{k}/b, \omega/b^z). \tag{3.16}$$

   with free parameters χ and z.

4. **RG flow**: Comparing the equations of motion for h_R and for h, one can derive the **RG equation** $\boldsymbol{K}_b = R_b(\boldsymbol{K})$.

5. **Fixed point**: The fixed point condition $\boldsymbol{K}^* = R_b(\boldsymbol{K}^*)$ determines the scaling exponents z and χ describing the long time and long distance scaling behavior.

The coarse-graining is the hardest step in the RG transformation. We will adopt the **perturbative RG** scheme where the coarse-graining is carried out perturbatively as a series in λ.

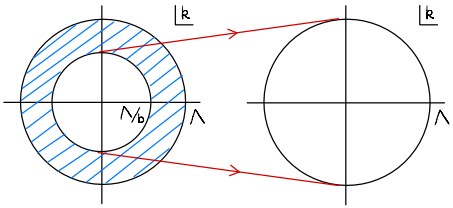

Figure 3.2: Momentum shell RG procedure.

3.5 Coarse graining

An integration over a momentum variable $\mathsf{p} = (\boldsymbol{k}, \omega)$ can be split into $\int đ\mathsf{p} = \int đ\omega \left(\int_{\partial\Lambda} đ\boldsymbol{k} + \int_{\mathring{\phi}\Lambda} đ\boldsymbol{k} \right)$. To distinguish diagrams associated with $\boldsymbol{k} \in \mathring{\phi}\Lambda$ and $\boldsymbol{k} \in \partial\Lambda$, we will add a slash to the latter. Then, the equations of motion for $h_<(\mathsf{p})$ and $h_>(\mathsf{p})$ have the diagramatic representation as shown in Fig. 3.3.

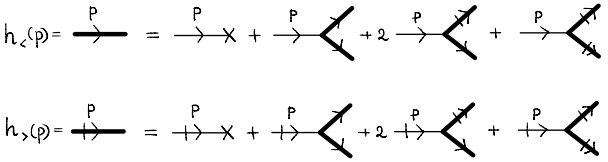

Figure 3.3: KPZ equation for $h_<$ and $h_>$.

Diagrams for $h_>$ include $h_>$ itself. Successive iterations then lead to the perturbation series for $h_>$. Upon iteration, the number of vertices remains the same or increases by one. Thus, n iteration yields the perturbative solution for $h_>$ which is exact up to $O(\lambda^n)$. Figure 3.4 shows the solution for $h_>$ up to $O(\lambda^2)$.

Plugging these diagrams into the equation of motion for $h_<$,

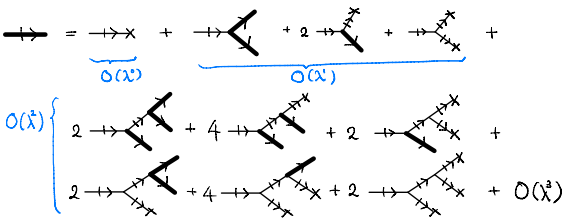

Figure 3.4: $h_>(\mathsf{p})$ up to $O(\lambda^2)$.

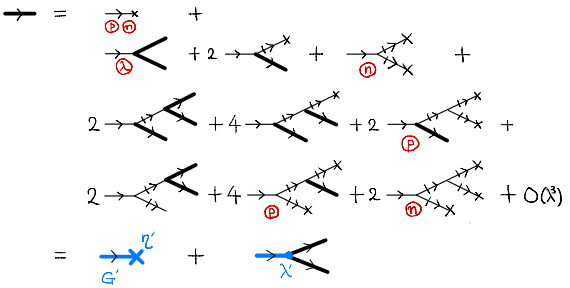

Figure 3.5: Effective equation of motion for $h_<$ up to $O(\lambda^2)$. The diagrams will be rearanged to have the form of the KPZ equation with the renormalized propagator G', noise η', and nonlinear coupling constant λ'. Diagrams contributing to the effective propagator, noise, and nonlinear coupling are marked with $\textcircled{p}$, $\textcircled{n}$, and $\textcircled{\lambda}$, respectively.

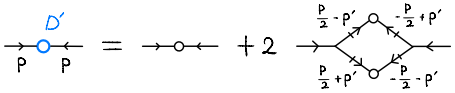

Figure 3.6: Renormalization diagram for the noise strength.

one obtains the effective equation of motion for $h_<$. It is presented in Fig. 3.5. The diagrams will be rearranged to find the effective propagator G', the effective noise η', and the effective nonlinear coupling strength λ'. One also needs the diagrams of the order of $O(\lambda^3)$ for λ', which are omitted in Fig. 3.5.

3.5.1 Effective noise $\eta'(\mathsf{p})$

The three diagrams marked with ⓝ in Fig. 3.5 include only propagators and noises. Thus, their sum, denoted as $\Sigma_\eta(\mathsf{p})$, is equal to $G_0(\mathsf{p})\eta'(\mathsf{p})$. The effective noise amplitude $D'(\mathsf{p})$ is defined by

$$\langle \Sigma_\eta(\mathsf{p})\Sigma_\eta(\mathsf{p}')\rangle = G_0(\mathsf{p})G_0(\mathsf{p}')D'(\mathsf{p})\,\delta(\mathsf{p}+\mathsf{p}'). \tag{3.17}$$

The contraction is represented by the diagram in Fig. 3.6 up to $O(\lambda^2)$, which yields

$$\begin{aligned} D'(\mathsf{p}) =& D + 2\left(-\frac{\lambda D}{2}\right)^2 \int_{\partial\Lambda} đ\boldsymbol{k}' \int đ\omega' \left(\frac{k^2}{4} - k'^2\right)^2 \times \\ & \left| G_0\left(\frac{\boldsymbol{k}}{2} - \boldsymbol{k}', \frac{\omega}{2} - \omega'\right) G_0\left(\frac{\boldsymbol{k}}{2} + \boldsymbol{k}', \frac{\omega}{2} + \omega'\right)\right|^2 + O(\lambda^4). \end{aligned} \tag{3.18}$$

The coarse-grained noise becomes colored whilst the bare noise is white. Since we are interested in the long time and long distance property, we approximate the noise as a white

noise whose strength is given by the value $D' = D'(\mathsf{p}{=}0)$ at zero momentum. The integral in (3.18) can be evaluated analytically d. When $b = e^{\delta s}$ with infinitesimal δs, it is given by

$$D' \simeq D\left(1 + \frac{D\lambda^2}{8\nu^3} K_d \delta s\right) + O(\lambda^4), \tag{3.19}$$

where K_d is a non-universal constant depending on d and Λ.

3.5.2 Effective propagator $G'(\mathsf{p})$

As evident from Fig. 3.5, the effective propagator G' is the response function of the field to the effective noise:

$$G'(\mathsf{p}) = \left\langle \frac{\delta h^<(\mathsf{p})}{\delta \eta'(\mathsf{p})} \right\rangle_\eta . \tag{3.20}$$

In addition to the diagrams $\Sigma_\eta = G_0\eta'$, the diagrams marked with ⓟ in Fig. 3.5 also contribute to the propagator. The renormalized propagator G' has the diagram representation as shown in Fig. 3.7. It is given by

$$\begin{aligned}\frac{G'(\mathsf{p})}{G_0(\mathsf{p})} =& 1 + 4G_0(\mathsf{p})\left(-\frac{\lambda}{2}\right)^2 D \int_{\partial\Lambda} đ\boldsymbol{k}' \int đ\omega' \\ & \left\{\left(\frac{\boldsymbol{k}}{2} - \boldsymbol{k}'\right)\cdot\left(\frac{\boldsymbol{k}}{2} + \boldsymbol{k}'\right)\right\}\left\{\left(-\frac{\boldsymbol{k}}{2} - \boldsymbol{k}'\right)\cdot\boldsymbol{k}\right\} \\ & G_0\left(\frac{\boldsymbol{k}}{2} - \boldsymbol{k}', \frac{\omega}{2} - \omega'\right)\left|G_0\left(\frac{\boldsymbol{k}}{2} + \boldsymbol{k}', \frac{\omega}{2} + \omega'\right)\right|^2 + O(\lambda^4)\end{aligned} \tag{3.21}$$

Note that the second ⓟ diagram in Fig. 3.5 vanishes identically due to the momentum conservation.

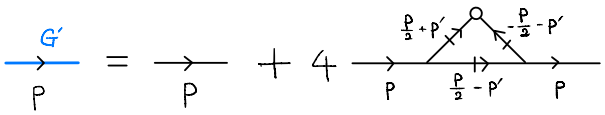

Figure 3.7: Renormalization diagram for the propagator.

The integral can be evaluated analytically near $\boldsymbol{k} = 0$ and $\omega = 0$. It is given by

$$G'(\boldsymbol{k}, 0) = \frac{1}{\nu' k^2} = G_0(\boldsymbol{k}, 0) \left[1 + \frac{D\lambda^2 (d-2) K_d}{8 d \nu^3} \delta s + O(k^2, \omega^2, \lambda^4) \right]. \tag{3.22}$$

Thus, the parameter ν renormalizes to

$$\nu' = \nu \left(1 - \frac{D\lambda^2 (d-2)}{8 d \nu^3} K_d \delta s \right). \tag{3.23}$$

where $b = e^{\delta s}$ with infinitesimal δs.

3.5.3 Effective nonlinear coupling λ'

In Fig. 3.5, diagrams contributing to the renormalization of λ are marked with $\textcircled{\lambda}$. Nontrivial diagrams appear at the order of $O(\lambda^3)$. Diagrams renormalizing λ' up to $O(\lambda^3)$ are presented in Fig. 3.8. The expression for λ' also depends on momenta of emanating edges. The long time and long distance behavior is dominated by the value at zero momentum. A straightforward algebra yields all the higher order diagrams are summed up to zero and only the bare diagram survive. Thus,

$$\lambda' = \lambda. \tag{3.24}$$

It is not an accidental coincidence but the consequence of the Gallilean invariance of the KPZ equation [KPZ86].

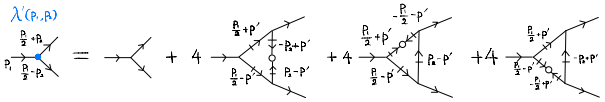

Figure 3.8: Renormalization diagrams for λ'.

3.6 RG flow equation

The RG transformation is completed by rescaling. We have already learned how the parameters are modified under rescaling. Applyinig Eq. (3.6) to ν', D', λ', we finally obtain the RG equation

$$\nu_b = b^{z-2}\nu', \quad D_b = b^{z-d-2\chi}D', \quad \lambda_b = b^{\chi+z-2}\lambda'. \tag{3.25}$$

For infinitesimally small δs ($b = e^{\delta s}$), the RG equation can be written in the differential equation form. They are given by

$$\begin{aligned}
\frac{d\nu}{ds} &= \lim_{\delta s\to 0}\frac{\nu_{b=e^{\delta l}} - \nu}{\delta s} = \left(z - 2 - \frac{(d-2)D\lambda^2}{8d\nu^3}K_d\right)\nu \\
\frac{dD}{ds} &= \left(z - d - 2\chi + \frac{D\lambda^2}{8\nu^3}K_d\right)D \\
\frac{d\lambda}{ds} &= (\chi + z - 2)\,\lambda.
\end{aligned} \tag{3.26}$$

3.7 Fixed point at $d = 1$

The fixed point condition for λ yields the scaling relation

$$\chi + z = 2. \tag{3.27}$$

To find χ and z, we need to know the fixed point value of $\bar{\lambda} \equiv \sqrt{DK_d\lambda^2/\nu^3)}$. Combining the RG equation in Eq. (3.26), we obtain

$$\frac{d\bar{\lambda}}{ds} = B(\bar{\lambda}) = \left(\frac{2-d}{2}\right)\bar{\lambda} + \left(\frac{2d-3}{8d}\right)\bar{\lambda}^3. \tag{3.28}$$

The flow function B is plotted in Fig. 3.9. When $d > 2$, the EW fixed point at $\bar{\lambda} = 0$ is a stable fixed point. The nonlinearity is irrelevant at the EW fixed point. In addition to the stable EW point, there is an unstable fixed point (open circular symbol). It raises a question whether there exists a strong coupling KPZ fixed point at dimensions $d > 2$. This issue is beyond the scope of the perturbative RG approach.

When $d < 3/2$, the EW point is unsable and there appears the stable KPZ fixed point (red circular symbol) at

$$\bar{\lambda}^* = \sqrt{4d(2-d)/(3-2d)}. \tag{3.29}$$

The scaling exponents at the KPZ fixed point are

$$\begin{aligned} z_{KPZ} &= 2 - \frac{2-d}{8d}(\bar{\lambda}^*)^2 = 2 - \frac{(2-d)^2}{2(3-2d)} \\ \chi_{KPZ} &= 1 - \frac{d}{2} + \frac{(d-1)}{8d}(\bar{\lambda}^*)^2 = 1 - \frac{d}{2} + \frac{(d-1)(2-d)}{2(3-2d)}. \end{aligned} \tag{3.30}$$

In particular, at $d = 1$, the scaling exponents at the KPZ fixed point are given by

$$z_{KPZ} = \frac{3}{2}, \quad \chi_{KPZ} = \frac{1}{2}\,. \tag{3.31}$$

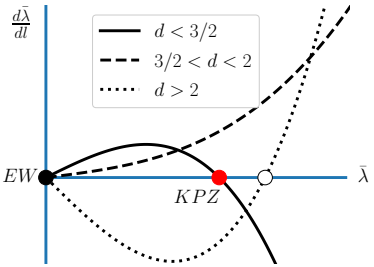

Figure 3.9: RG flow of $\bar{\lambda}$.

4

Momentum shell RG for the ϕ^4 theory

This chapter covers the renormalization group transformation for the ϕ^4 **theory** in the d-dimensional continuum space. The ϕ^4 theory for a continuos field $\phi(\boldsymbol{r})$ in volume V is defined by the Hamiltonian

$$\mathcal{H}[\phi(\boldsymbol{r})] = \beta H[\phi(\boldsymbol{r})] = \int_V d^d\boldsymbol{r} \left[\frac{1}{2}|\nabla\phi|^2 + \frac{1}{2}u_2\phi^2 + \frac{1}{4}u_4\phi^4 - h\phi\right] \tag{4.1}$$

with the partition function

$$Z(u_2, u_4, h; V) = \int [\mathcal{D}\phi] e^{-\mathcal{H}[\phi(\boldsymbol{r})]}. \tag{4.2}$$

It is customary to set the coefficient of the gradient term to a constant value $1/2$ redefining the field variable. One may call $\mathcal{H}$ an effective Hamiltonian or an action. One can derive this form of the action from a microscopic model system on a discrete lattice by using the **Hubbard-Stratonotovich transformation**. We refer the readers to *(Exercise 3-3)* and *(Exercise 6-3)* of Ref. [Gol92].

The **Ginzburg-Landau theory** ignores any thermal fluctuations and approximates the path integral in (4.2) with the ex-

tremal value at the optimal field $\bar{\phi}(\boldsymbol{r})$ satisfying

$$-\nabla^2\bar{\phi}(\boldsymbol{r}) + u_2\bar{\phi}(\boldsymbol{r}) + u_4\bar{\phi}^3(\boldsymbol{r}) - h(\boldsymbol{r}) = 0. \tag{4.3}$$

When the magnetic field is uniform $h(\boldsymbol{r}) = h$, it reduces to the **mean field theory** with

$$u_2\bar{\phi} + u_4\bar{\phi}^3 = h. \tag{4.4}$$

If one takes into account the fluctuations around the optimal fields uo to the second order in $\delta\phi(\boldsymbol{r}) = \phi(\boldsymbol{r}) - \bar{\phi}(\boldsymbol{r})$, then it reduces to the **Gaussian model**. All these approximate theories belong to the **mean field universality class** and fail to describe the correct critical phenomena in dimensions below the **upper critical dimension** $d_u = 4$.

4.1 Power counting and dimensional analysis

The action $\mathcal{H}$ in Eq. (4.1) is dimensionless. Using this, one finds the dimensions of the field ϕ and the coupling constants in terms of the powers of length L:

$$[\boldsymbol{r}] = L^1,\ [\phi] = L^{1-d/2},\ [u_2] = L^{-2},\ [u_4] = L^{d-4},\ [h] = L^{-(1+d/2)}. \tag{4.5}$$

The dimensional analysis reveals how the system transforms under the **simple rescaling** (*RG without coarse graining*)

$$\boldsymbol{r} \to \boldsymbol{r}' = \boldsymbol{r}/b, \quad \phi(\boldsymbol{r}) \to \phi'(\boldsymbol{r}') = b^{-1+d/2}\phi(\boldsymbol{r}). \tag{4.6}$$

Changing the variables in Eq. (4.2), one finds that

$$Z(u_2, u_4, h; V) = Z(b^2u_2, b^{4-d}u_4, b^{1+d/2}h; V/b^d). \tag{4.7}$$

up to a constant.

When $d > d_u = 4$, the quartic term, which vanishes as the scale factor b grow, is **irrelevant**. Thus, the ϕ^4 field theory becomes equivalent to the Gaussian field theory and the mean field theory becomes exact. On the contrary, when $d < d_u$, the quartic term is a **relevant** perturbation to the Gaussian field theory. The simple rescaling does not provide any useful information on the critical behavior.

4.2 Momentum shell RG

It is convenient to work in the Fourier space:

$$\begin{aligned} \phi(\boldsymbol{r}) &= \int^{\Lambda} đ\boldsymbol{k}\ \varphi(\boldsymbol{k}) e^{i\boldsymbol{k}\cdot\boldsymbol{r}}, \\ \varphi(\boldsymbol{k}) &= \int d^d\boldsymbol{r}\ \phi(\boldsymbol{r}) e^{-i\boldsymbol{k}\cdot\boldsymbol{r}} = \varphi(-\boldsymbol{k})^*, \end{aligned} \tag{4.8}$$

where $\int^{\Lambda} đ\boldsymbol{k}$ denotes the integration within the ultraviolet cutoff $\Lambda = 2\pi/a_0$. Since $\phi(\boldsymbol{r})$ is a real field, $\varphi(-\boldsymbol{k}) = \varphi(\boldsymbol{k})^*$. The action is written as

$$\begin{aligned} \mathcal{H}[\varphi] = \int^{\Lambda} đ\boldsymbol{k}\ \left[\frac{1}{2}(k^2 + u_2)|\varphi(\boldsymbol{k})|^2\right] \\ + \frac{u_4}{4}\int_{1,2,3,4}^{\Lambda} \varphi_1\varphi_2\varphi_3\varphi_4\, \tilde{\delta}(\boldsymbol{k}_1 + \boldsymbol{k}_2 + \boldsymbol{k}_3 + \boldsymbol{k}_4), \end{aligned} \tag{4.9}$$

where we used the shorthand notation

$$\int_i = \int đ\boldsymbol{k}_i = \int \frac{d^d\boldsymbol{k}_i}{(2\pi)^d} \text{ and } \varphi_i = \varphi(\boldsymbol{k}_i). \tag{4.10}$$

The momentum shell RG proceeds in the following procedure:

1. Introduce a scale factor b and separate the field $\varphi(\boldsymbol{k})$ into the long and short wavelength components.

$$\varphi(\boldsymbol{k}) = \begin{cases} \varphi_l(\boldsymbol{k}) & \text{for } \boldsymbol{k} \in \bar{\partial}\Lambda \ (|\boldsymbol{k}| < \Lambda/b) \\ \varphi_s(\boldsymbol{k}) & \text{for } \boldsymbol{k} \in \partial\Lambda \ (\Lambda/b < |\boldsymbol{k}| < \Lambda) \end{cases} \tag{4.11}$$

2. **(Coarse graining)** Perform the partial integration over φ_s in the momentum shell $\partial\Lambda$ to derive the effective action $\mathcal{H}'$ for φ_l.

$$e^{-\mathcal{H}'[\varphi_l]} = \int [\mathcal{D}\varphi_s] e^{-\mathcal{H}[\varphi_l + \varphi_s]}. \tag{4.12}$$

   The coarse-graining yields effective coupling constants

$$u_2' = f_2(u_2, u_4; b), \quad u_4' = f_4(u_2, u_4; b), \quad h' = f_h(h; b). \tag{4.13}$$

3. **(Rescaling)** Rescale the momentum variable $\boldsymbol{k} \to \boldsymbol{k}_R = b\boldsymbol{k}$ and the field $\varphi_l(\boldsymbol{k}) \to \varphi_R(\boldsymbol{k}_R) = z_b^{-1}\varphi_l(\boldsymbol{k}_R/b)$ to complete the RG transformation. This procedure is the same as the power counting or the dimensional analysis.

4. **(RG equation)** Combining the coarse-graining and the rescaling, one finally obtain the RG equation

$$u_{2,b} = b^2 u_2', \quad u_{4,b} = l^{4-d} u_4', \quad h_b = l^{1+d/2} h'. \tag{4.14}$$

5. Draw the **RG flow** and find the **fixed points** and **relevant scaling variables** and **scaling exponents**.

In this lecture, we focus on the case without external magnetic field.

4.3 Perturbative expansion for coarse graining $(h = 0)$

The coarse-graining of (4.12) is the hardest task in the RG calculations. It demands some mathematical techniques such as the **diagram expansion**, **linked cluster theorem**, **Wick's theorem**, and so on. These techniques are repeatedly used in the analytic calculations. This section may be useful for those who are interested in the analytic methods.

The action in Eq. (4.9) is the sum of three terms:

$$\mathcal{H} = \mathcal{H}_{0,l}[\varphi_l] + \mathcal{H}_{0,s}[\varphi_s] + V[\varphi_s; \varphi_l] \tag{4.15}$$

where

$$\begin{aligned} \mathcal{H}_{0,l}[\varphi_l] &= \int^{\Lambda/l} đ\boldsymbol{k} \left[\frac{1}{2}(k^2 + u_2)|\varphi_l(\boldsymbol{k})|^2\right] \\ \mathcal{H}_{0,s}[\varphi_s] &= \int_{\partial\Lambda} đ\boldsymbol{q} \left[\frac{1}{2}(q^2 + u_2)|\varphi_l(\boldsymbol{q})|^2\right] \end{aligned} \tag{4.16}$$

are the **Gaussian (free) Hamiltonian** for the long and short wavelength components, and $V[\varphi_s; \varphi_l] = O(u_4)$ is the ϕ^4 term. The renormalized action is then written as

$$\begin{aligned} e^{-\mathcal{H}'[\varphi_l]} &= Z_{0,s} e^{-\mathcal{H}_{0,l}[\varphi_l]} \int [\mathcal{D}\varphi_s] e^{-V[\varphi_s;\varphi_l]} \frac{1}{Z_{0,s}} e^{-\mathcal{H}_{0,s}[\varphi_s]} \\ &= Z_{0,s} e^{-\mathcal{H}_{0,l}[\varphi_l]} \left\langle e^{-V[\varphi_s;\varphi_l]} \right\rangle_s, \end{aligned} \tag{4.17}$$

where $Z_{0,s} = \int [\mathcal{D}\varphi_s] e^{-\mathcal{H}_{0,s}[\varphi_s]}$ is the partition function for the Gaussian model for φ_s. It only contribute to the analytic part of the free energy and does not renormalize any coupling constants. It will be ignored. $\langle() \rangle_s$ stands for the canonical ensemble average with respect to the Gaussian Hamiltonian $\mathcal{H}_{0,s}$. The

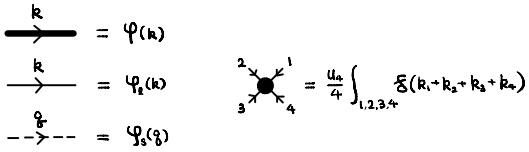

Figure 4.1: Diagram rules

renormalized Hamiltonian is given by

$$\mathcal{H}'[\varphi_l] = \mathcal{H}_{0,l}[\varphi_l] - \ln\left\langle e^{-V[\varphi_s;\varphi_l]}\right\rangle_s . \tag{4.18}$$

4.3.1 Cumulant expansion

In principle, the ensemble average over the Gaussian Hamiltonian can be evaluated. However, since e^{-V} is highly nonlinear, the closed form expression for $\left\langle e^{-V}\right\rangle_s$ is not available. Thus, we rely on the cumulant expansion

$$\ln\left\langle e^{-V}\right\rangle_s = -\langle V\rangle_s + \frac{1}{2}\left(\langle V^2\rangle_s - \langle V\rangle_s^2\right) + \cdots , \tag{4.19}$$

wich is equivalent to the series expansion in u_4.

4.3.2 Diagram method

Expressions for $\langle V^n\rangle_s$ are too lengthy to manupulate. The diagram method is an efficient way to handle such complicated expressions. We introduce the rule depicted in Fig. 4.1: (i) A **thick line** corresponds to a field variable $\varphi(\boldsymbol{k})$. It is associated with a momentum variable, which may be omitted or written explicitly with an arrow. If $\boldsymbol{k} \in \hat{\partial}\Lambda$, the field variable is represented

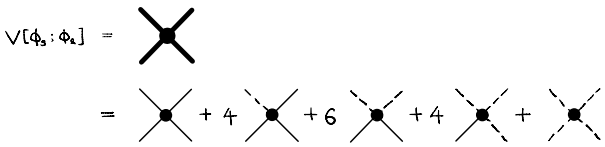

Figure 4.2: Diagram representation of $V[\varphi_s; \varphi_l]$.

with a **thin line**. If $\boldsymbol{k} \in \partial\Lambda$, the field variable is represented with a **dashed line**. (ii) A **four-vertex** means the integration over all incoming momentum variables adding up to zero (**momentum conservation**) with the amplitude $u_4/4$.

Using these rules, $V[\varphi_s; \varphi_l]$ is represented with the diagram in Fig. 4.2. Note that a thick line (φ) attached to a four-vertex can be either a thin line (φ_l) or a dashed line (φ_s). Thus, the original diagram is the sum of 16 diagrams, which are grouped into five independent diagrams.

4.3.3 Gaussian average and Wick's theorem

For the cumulants of V, we need to evaluate the correlation functions $\langle \varphi_s(\boldsymbol{q}_1) \cdots \varphi_s(\boldsymbol{q}_n) \rangle_s$ with respect to the Gaussian Hamiltonian $\mathcal{H}_{0,s}$ in Eq. (4.16). A correlation function of odd number of fields is identically zero. The 2-point correlation function is given by

$$C(\boldsymbol{q}_1, \boldsymbol{q}_2) \equiv \langle \varphi_s(\boldsymbol{q}_1) \varphi_s(\boldsymbol{q}_2) \rangle_s = \delta(\boldsymbol{q}_1 + \boldsymbol{q}_2) G_0(\boldsymbol{q}_1) \tag{4.20}$$

where

$$G_0(\boldsymbol{q}) = \frac{1}{q^2 + u_2^2}. \tag{4.21}$$

is called the **free propagator**.

Figure 4.3: Diagramatic rule for contraction

A $(2n)$-point correlation function is given by a combination of free propagators. The **Wick's theorem** states that it is the sum, over all ways pairing up of $2n$ fields into n pairs [**contraction**], of the products of pairwise two-point correlation functions. For example,

$$\begin{aligned}\langle \varphi_s(1)\varphi_s(2)\varphi_s(3)\varphi_s(4)\rangle_s =& C(1,2)C(3,4) + C(1,3)C(2,4) \\ &+ C(1,4)C(2,3).\end{aligned} \tag{4.22}$$

We have already seen this this example in the discussion of the KPZ system.

In a diagram method, the free propagator is represented with a thin line. A propagator line should not be confused with a field line. A propagator appears when two fields are contracted. Thus, both ends of a propagator line are attached to a vertex. On the other hand, one end of a field line is attached to a vertex and another end is free. Figure 4.3 illustrates the diagram rule for contraction.

4.4 Feynman rule for the coarse-graining

One can perform the coarse-graining by enumerating all the cases where thick field lines (φ) are replaced with thin field lines (φ_l) and dashed field lines (φ_s). We have done this in the analysis of the KPZ equation. Careful readers may realize that

such an enumeration is in fact unneccessary when one evaluates the Gaussian average of the nth cumulant of V. It suffices to contract any pairs of field lines directly by joining them to form a propagator line. Remaining uncontracted edges should be regarded as the field lines φ_l. Here is the concise rule for the nth order cumulant of V:

1. Draw n vertices . Each vertex has four edges.

2. Among $4n$ edges, pair up some of them and contract the pairs. A contracted (uncontracted) edge will be called an **internal (external) edge**. Contraction patterns of the **same topology** contribute the same weight to the cumulants. Thus, it is wise to find the set of topologically distinct contraction patterns and their **degeneracy**. According to the **linked cluster theorem**, only **connected diagrams** conribute to the cumulant. **Disconnected diagrams** do not contribute to the commulant and should be ignored.

3. A weight of a contraction pattern is obtained by replacing an internal edge with a free propagator $G_0(\boldsymbol{q} \in \partial\Lambda)$ and an external edge with a field $\varphi_l(\boldsymbol{k} \in \partial\Lambda)$ and integrating over all internal momenta $\boldsymbol{q}$'s. Each vertex is assigned to a factor $(u_4/4)$ and imposes the momentum conservation.

4. The cumulant is then given by the sum of the weights of all contraction-generated connected diagrams.

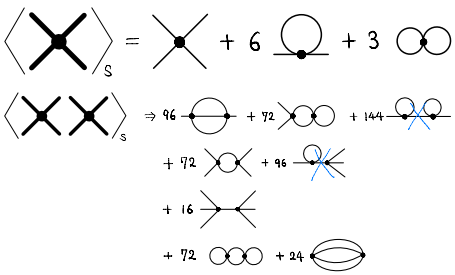

Figure 4.4: Diagrams for the first and the second order cumulants of V.

4.5 Cumulants of V

We are now ready to calculate the cumulants of $V[\varphi_s; \varphi_l]$. The diagrams for the first and second order cumulants are given in Fig. 4.4. The diagrams with two (four) external edges renormalize u_2 (u_4). Those with no external edges contribute to the non-singular part of the free energy density and do not renormalize any coupling constants. There appears a diagram with six external edges, which corresponds to a ϕ^6 term. Higher order non-linear terms are generated under the RG. The dimensional analysis tells us that ϕ^6 terms or higher order terms are less relevant to the ϕ^4 term. As far as the critical behavior is concerned, we can ignore the RG-generated higher order terms. Note that two diagrams in Fig. 4.4 vanish because they are not consistent with the momentum conservation.

The diagrams are evaluated to yield the renormalized action

$$\begin{aligned}\mathcal{H}'[\varphi_l] = &\int_{\hat{\phi}\Lambda} đ\boldsymbol{k}\frac{1}{2}(k^2+u_2^2)|\varphi_l(\boldsymbol{k})|^2 \\ &+ 6\frac{u_4}{4}\left(\int_{\hat{\phi}\Lambda} đ\boldsymbol{k}|\varphi_l(\boldsymbol{k})|^2\right) I_1(u_2;b) \\ &+ \frac{u_4}{4}\int_{1,2,3,4\in\hat{\phi}\Lambda} \varphi_l^{(1)}\varphi_l^{(2)}\varphi_l^{(3)}\varphi_l^{(4)}\,\delta_{1,2,3,4} \\ &- 36\left(\frac{u_4}{4}\right)^2\int_{1,2,3,4\in\hat{\phi}\Lambda} \varphi_l^{(1)}\varphi_l^{(2)}\varphi_l^{(3)}\varphi_l^{(4)}\,\delta_{1,2,3,4} I_2(u_2;1,2,b),\end{aligned} \tag{4.23}$$

where

$$\begin{aligned} I_1(u_2;b) &= \int_{\partial\Lambda} đ\boldsymbol{q} G_0(\boldsymbol{q}) \\ I_2(u_2;\boldsymbol{k},\boldsymbol{k}',b) &= \int_{\partial\Lambda} đ\boldsymbol{q} G_0(\boldsymbol{q}) G_0(\boldsymbol{k}+\boldsymbol{k}'-\boldsymbol{q}).\end{aligned} \tag{4.24}$$

It is evident that the diagram with I_1 renormalizes u_2. The diagram with I_2 renormalizes u_4 with a momentum dependent factor. The large length scale property is dominated by the couplings at zero momentum. So, we will keep only the zero momentum component

$$I_2(u_2;b) = I_2(u_2;\boldsymbol{k}_1=0,\boldsymbol{k}_2=0;b). \tag{4.25}$$

The coarse-graining renormalizes the coupling constants as

$$\begin{aligned} u_2' &= u_2 + 3u_4 I_2(u_2;b) + O(u_4^2) \\ u_4' &= u_4\left(1 - 9u_4 I_2(u_2;b) + O(u_4^2)\right).\end{aligned} \tag{4.26}$$

4.6 RG equation

The RG transformation is completed by rescaling the momentum and the field variable. The coupling constants acquire the factor obtained in the dimensional analysis. Therefore, we finally obtain the RG flow equations:

$$\begin{aligned} u_2 &\xrightarrow{\text{coarse-graining}} u_2' \xrightarrow{\text{rescaling}} u_2(b) = b^2 u_2' \\ u_4 &\xrightarrow{\text{coarse-graining}} u_4' \xrightarrow{\text{rescaling}} u_4(b) = b^{4-d} u_4'. \end{aligned} \tag{4.27}$$

It is convenient to consider the RG equation in the **differential form**. Let the scale factor $b = e^{\delta s}$ with an infinitesimal *logarithmic scale factor* δs. Then,

$$\begin{aligned} I_1 &= \int_{\Lambda e^{-\delta s}}^{\Lambda} dq \frac{K_d q^{d-1}}{q^2 + u_2} \simeq \frac{K_d \Lambda^d}{\Lambda^2 + u_2} \delta s \\ I_2 &\simeq \frac{K_d \Lambda^d}{(\Lambda^2 + u_2)^2} \delta s \end{aligned} \tag{4.28}$$

where $K_d \equiv S_{d-1}/(2\pi)^d$ with $S_{d-1} = 2\pi^{d/2}/\Gamma(d/2)$ the surface area of the unit d-sphere. The differential RG flow equation is given by

$$\begin{aligned} \frac{du_2}{ds} &= 2u_2 + \frac{3K_d \Lambda^d}{\Lambda^2 + u_2} u_4 + O(u_4^2) \\ \frac{du_4}{ds} &= u_4 \left((4-d) - \frac{9K_d \Lambda^d}{(\Lambda^2 + u_2)^2} u_4 + O(u_4^2) \right). \end{aligned} \tag{4.29}$$

4.7 Fixed points and ϵ-expansion

The RG flow equation in (4.29) predicts two fixed points: one at $u_4^* = 0$ and another at $u_4^* \simeq (4-d)(\Lambda^2 + u_2^*)^2/(9K_d\Lambda^4)$. The

result of the perturbative RG is meaningful when the magnitude of u_4^* is small. Thus, we expect that the perturbative RG becomes accurate when the spatial dimensionality is close to the upper critical dimension $d_u = 4$.

Let $\epsilon \equiv 4 - d$. The fixed points are located at

$$(u_2^*, u_4^*) = \begin{cases} (0,0) & \textbf{(Gaussian)} \\ \left(-\frac{\Lambda^2}{6}\epsilon, \frac{1}{9K_4}\epsilon\right) + O(\epsilon^2) & \textbf{(Wilson-Fisher)} \end{cases} \tag{4.30}$$

The Gaussian model appears as a fixed point of the RG transformation. In addition, there emerges a non-Gaussian fixed point with $u_4^* = O(\epsilon^1)$, which is called the Wilson-Fisher fixed point [1]. The RG flow equation linearized around the fixed points are

$$\begin{aligned} \frac{d}{ds}\begin{pmatrix}\delta u_2 \\ \delta u_4\end{pmatrix} &= \begin{pmatrix} 2 & 3K_4\Lambda^2 \\ 0 & \epsilon \end{pmatrix}_G \begin{pmatrix}\delta u_2 \\ \delta u_4\end{pmatrix} \\ \frac{d}{ds}\begin{pmatrix}\delta u_2 \\ \delta u_4\end{pmatrix} &= \begin{pmatrix} 2 - \frac{\epsilon}{3} & 3K_4\Lambda^2(1+\epsilon/6) \\ 0 & -\epsilon \end{pmatrix}_{WF} \begin{pmatrix}\delta u_2 \\ \delta u_4\end{pmatrix}, \end{aligned} \tag{4.31}$$

where $()_G$ and $()_{WF}$ are the linearize RG matrix at the Gaussian and the Wilson-Fisher fixed points, respectively. The diagonal elements are the scaling dimensions of the scaling fields δu_2 and $\delta \tilde{u}_4$ (linear combination of δu_2 and δu_4). The scaling exponents are given by

$$\begin{aligned} (y_2, y_4) &= (2, \epsilon) \quad \text{at the Gaussian f.p.} \\ &= (2 - \frac{\epsilon}{3}, -\epsilon) \quad \text{at the Wilson-Fisher f.p.} \end{aligned} \tag{4.32}$$

The schematic RG flow in the parameter space is presented in Fig. 4.5.

[1] Higher order cumulant expansions lead to the ϵ-expansion to higher order.

Note that the sign of y_4 changes as the sign of ϵ changes. The nature of the phase transition also changes accordingly:

- $d < 4$: The quartic term is relevant and makes the Gaussian fixed point unstable. The system undergoes a phase transition as one crosses the **critical manifold** flowing into the Wilson-Fisher fixed point. The critical behavior is therfore determined by the scaling exponents at the Wilson-Fisher fixed point. The temperature-like scaling variable $\delta u_2 = u_2 - u_2^*$ is **relevant** with the scaling dimension $y_t = y_2 = 2 - \epsilon/3 + O(\epsilon^2)$. The scaling dimension of the magnetic field is given by $y_h = 2 - \epsilon/2 + O(\epsilon^2)$.
- $d > 4$: The quartic term is irrelevant and the Gaussian fixed point is stable against the quartic term. The critical manifold flows into the Gaussian fixed point. Thus, the critical behavior is governed by the Gaussian fixed point. The scaling dimensions are given by the mean field value $y_t = 2$ and $y_h = 3$.

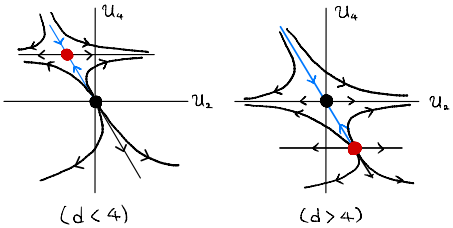

Figure 4.5: RG flow of the ϕ^4 model in dimensions below and above the upper critical dimension $d_u = 4$. The Wilson-Fisher (Gaussian) fixed points are marked with red (black) dots. The critical manifolds separating the ordered and the disordered phases are drawn with blue lines.

Bibliography

[Gol92] Nigel Goldenfeld. *Lectures on phase transitions and the renormalization group*. Addison-Wesley. Addison-Wesley, 1992.

[Kad66] Leo P Kadanoff. Scaling laws for ising models near T_c. *Physics Physique Fizika*, 2(6):263–272, 1966.

[KG81] Miron Kaufman and Robert B. Griffiths. Exactly soluble Ising models on hierarchical lattices. *Physical Review B*, 24(1):496–498, 1981.

[KPZ86] Mehran Kardar, Giorgio Parisi, and Yi-Cheng Zhang. Dynamic Scaling of Growing Interfaces. *Physical Review Letters*, 56(9):889–892, 1986.

[MHKZ89] E Medina, T Hwa, M Kardar, and Y C Zhang. Burgers equation with correlated noise: Renormalization-group analysis and applications to directed polymers and interface growth. *Physical Review A*, 39(6):3053, 1989.

[MM75] Shang-keng Ma and Gene F. Mazenko. Critical dynamics of ferromagnets in 6-ε dimensions: General discussion and detailed calculation. *Physical Review B*, 11(11):4077–4100, 1975.

[Wid65] B Widom. Equation of State in the Neighborhood of the Critical Point. *The Journal of Chemical Physics*, 43(11):3898–3905, 1965.